PAPER • OPEN ACCESS

Role of matrix elements in the time-resolved photoemission signal

New Journal of Physics
The open access journal at the forefront of physics

Deutsche Physikalische Gesellschaft DPG
IOP Institute of Physics

Published in partnership with: Deutsche Physikalische Gesellschaft and the Institute of Physics

OPEN ACCESS

RECEIVED
15 November 2019

REVISED
6 January 2020

ACCEPTED FOR PUBLICATION
22 January 2020

PUBLISHED
18 February 2020

PAPER

Role of matrix elements in the time-resolved photoemission signal

F Boschini[1,2], D Bugini[3,4], M Zonno[1,2], M Michiardi[1,2,5], R P Day[1,2], E Razzoli[1,2], B Zwartsenberg[1,2], M Schneider[1,2], E H da Silva Neto[1,2,6,7], S dal Conte[3], S K Kushwaha[8,9], R J Cava[8], S Zhdanovich[1,2], A K Mills[1,2], G Levy[1,2], E Carpene[10], C Dallera[3], C Giannetti[11,12], D J Jones[1,2], G Cerullo[3] and A Damascelli[1,2]

[1] Quantum Matter Institute, University of British Columbia, Vancouver, BC V6T 1Z4, Canada
[2] Department of Physics & Astronomy, University of British Columbia, Vancouver, BC V6T 1Z1, Canada
[3] Dipartimento di Fisica, Politecnico di Milano, I-20133 Milano, Italy
[4] Center for Nano Science and Technology@PoliMi, Istituto Italiano di Tecnologia, I-20133 Milano, Italy
[5] Max Planck Institute for Chemical Physics of Solids, Nöthnitzer Straße 40, Dresden, D-01187, Germany
[6] Max Planck Institute for Solid State Research, Heisenbergstrasse 1, D-70569 Stuttgart, Germany
[7] Department of Physics, University of California, Davis, CA 95616, United States of America
[8] Department of Chemistry, Princeton University, Princeton, NJ 08544, United States of America
[9] MPA-MAGLAB, Los Alamos National Laboratory, Los Alamos, NM 87504, United States of America
[10] IFN-CNR, Dipartimento di Fisica, Politecnico di Milano, I-20133 Milano, Italy
[11] Department of Mathematics and Physics, Università Cattolica del Sacro Cuore, Brescia, BS I-25121, Italy
[12] Interdisciplinary Laboratories for Advanced Materials Physics (ILAMP),Università Cattolica del Sacro Cuore, Brescia I-25121, Italy

E-mail: boschini@phas.ubc.ca **and** damascelli@physics.ubc.ca

Keywords: time- and angle-resolved photoemission spectroscopy (TR-ARPES), matrix-elements, topological insulators, ultrafast electron dynamics

Supplementary material for this article is available online

Abstract

Time- and angle-resolved photoemission spectroscopy (TR-ARPES) provides access to the ultrafast evolution of electrons and many-body interactions in solid-state systems. However, the momentum- and energy-resolved transient photoemission intensity may not be unambiguously described by the intrinsic relaxation dynamics of photoexcited electrons alone. The interpretation of the time-dependent photoemission signal can be affected by the transient evolution of the electronic distribution, and both the one-electron removal spectral function as well as the photoemission matrix elements. Here we investigate the topological insulator $Bi_{1.1}Sb_{0.9}Te_2S$ to demonstrate, by means of a detailed probe-polarization dependent study, the transient contribution of matrix elements to TR-ARPES.

1. Introduction

The development of pump-probe techniques has provided the opportunity to extend the study of solid state systems into the time domain, garnering important insights regarding transient phenomena in addition to new perspectives on persistent challenges from equilibrium [1]. Generally speaking, pump-probe techniques rely on a simple principle: a pump pulse drives the system out-of-equilibrium while a delayed probe pulse tracks intrinsic scattering properties on an ultrafast time scale.

The momentum information accessible to time- and angle-resolved photoemission spectroscopy (TR-ARPES) offers a significant advantage over other pump-probe techniques, as the modifications to the electronic structure and relaxation dynamics of photoexcited electrons are observed directly. TR-ARPES has been widely used to study the transient evolution of exotic phases in condensed matter as disparate as unconventional superconductivity [2–4], charge-order [5], excitonic condensates [6], and Floquet states [7, 8]. While the technique is by now fairly well-established, interpretation and analysis of TR-ARPES has yet to take advantage of the vast amount of information encoded in the experimental signal. Presently, it is conventional to emphasize the temporal evolution of the electronic temperature [4, 9–12] or the photoemission intensity in well-defined momentum-energy regions [13–16].

While in many cases this approach provides a basic understanding of some transient properties of the electronic population, a comprehensive description of the experiment is challenging.

To explore this further, we consider the form of the photoemission signal, for fixed energy ω and momentum $\mathbf{k}$, as it is defined via Fermi's Golden rule [17]

$$I_{\mathrm{PES}}(\omega, \mathbf{k}) = |M^{\mathbf{k}}_{\mathrm{f,i}}|^2 \cdot A(\omega, \mathbf{k}) \cdot \mathrm{f}(\omega, \mathbf{k}), \tag{1}$$

where $|M^{\mathbf{k}}_{\mathrm{f,i}}|^2$ is the photoemission matrix element, $A(\omega, \mathbf{k})$ the one-electron removal spectral function, and $f(\omega, \mathbf{k})$ the Fermi–Dirac distribution function. It is important to note that equation (1) is only strictly valid at equilibrium and may not describe completely the effect of the pump's electric field on a system's ground-state [18]. However, for time delays longer than the intrinsic thermalization time (tens-to-hundreds of fs depending on the system under consideration), the TR-ARPES signal for each time delay may be well approximated as a single-photon photoemission process from a thermally-broadened ground-state, i.e. equation (1) can be extended in the time domain τ. Within this approximation, the temporal evolution of $f(\omega, \mathbf{k}, \tau)$ describes the intrinsic relaxation processes for fixed ω and $\mathbf{k}$. In addition to $f(\omega, \mathbf{k}, \tau)$, much emphasis has also been placed on the evolution of $A(\omega, \mathbf{k}, \tau)$, which encodes information regarding the bare electronic dispersion [19, 20] and many-body interactions [21]. Such dynamical analysis of $A(\omega, \mathbf{k}, \tau)$ has been applied successfully to, for example, ultrafast metal–insulator transitions [5, 6, 22] as well as the quenching of phase coherence in superconducting condensates [2, 3]. To date however, the possible role of the time-dependent matrix element term $|M^{\mathbf{k}}_{\mathrm{f,i}}(\tau)|^2$ has been neglected in the analysis of TR-ARPES experiments, apart from sporadic theoretical investigations [23]. Derived from the matrix elements connecting the initial (i) and final (f) state of the photoemitted electron, $|M^{\mathbf{k}}_{\mathrm{f,i}}(\tau)|^2$ depends on the experimental geometry and orbital symmetry of the initial states. This term may be sensitive to modifications of both the electronic and lattice structures, influencing the orbital symmetry and complicating the interpretation of relaxation dynamics considerably. Note that for $\tau \gg 0$, i.e. when pump and probe pulses are not synchronous, intermediate and virtual state contributions to $|M^{\mathbf{k}}_{\mathrm{f,i}}(\tau)|^2$, which mediate two-photon-photoemission processes, can be neglected. The possibility that the temporal evolution of $A(\omega, \mathbf{k}, \tau)$, $f(\omega, \mathbf{k}, \tau)$, and $|M^{\mathbf{k}}_{\mathrm{f,i}}(\tau)|^2$ are intertwined raises important questions regarding the degree of confidence with which the ultrafast evolution of ARPES intensity can be associated with the intrinsic electronic relaxation dynamics alone.

To illustrate this point, figure 1(a) shows how a simulated transient increase of the matrix element $|M(\tau)|^2$ (blue line) may affect the extracted electron dynamics. The relaxation dynamics of electrons in the occupied states, i.e. below the E_{F}, are described by the evolution of the electronic distribution $f(\tau)$ (black line). When plotting the modeled transient photoemission intensity (red line, proportional to $f(\tau) \cdot |M(\tau)|^2$), we note that it overshoots its equilibrium value ($\tau < 0$) for late delays. This peculiar behavior may become manifest when the recovery time of $|M(\tau)|^2$ is longer than the one of $f(\tau)$ and may affect the interpretation and extraction of intrinsic relaxation times. This emphasizes the complications that can arise when the dynamical response of the matrix-element is neglected.

Such a scenario is not merely hypothetical: we provide here a real example of this complex co-evolution, observed in the relaxation dynamics of the topological insulator (TI) $Bi_{1.1}Sb_{0.9}Te_2S$ (BSTS) [24]. We demonstrate that the pump pulse drives a long-lasting ($\tau > 6$ ps) modification of the angular intensity distribution (i.e. matrix elements), as well as the band dispersion of the topological surface state (TSS). To extract the contribution of $|M(\tau)|^2$ to the observed ps thermalization dynamics, a polarization-dependent TR-ARPES study was conducted, elucidating the essential role of this term in the apparent relaxation dynamics of the electronic spectral function. While such a study is in principle possible in a variety of materials, TIs such as BSTS are ideally-suited to our purposes owing to their strong response to an infrared (IR) pump in terms of transient occupation of the TSS above the E_{F} [15, 16, 25–27], and susceptibility to the optical excitation of phonon modes [19]. BSTS is preferred in this particular case to Bi_2Se_3 and Bi_2Te_3 due to the high chemical stability of the surface and the large bulk conductivity gap, which facilitates consideration of the TSS in isolation from the bulk states.

2. Experimental

Pump-probe TR-ARPES experiments were conducted using a 1.55 eV pump and 6.2 eV probe beam (250 kHz repetition rate, 300 μm and 150 μm spot sizes, respectively), with photoemitted electrons collected via a hemispherical electron analyzer (SPECS Phoibos 150—overall momentum, energy and temporal resolutions are <0.003 Å^{-1}, 19 meV and 250 fs, respectively). The incident fluence of the s-polarized pump was 40 μJ cm^{-2} throughout this work for TR-ARPES measurements. Note that no pump-induced multi-photon effects have been detected at this fluence, and space-charge effects have been eliminated within our resolving power by reducing the probe flux (this is done by tracking the shift and broadening of the Fermi edge). BSTS samples (crystal growth details in [24]) were oriented via Laue diffraction, then cleaved and measured nominally at 6 K in vacuum better than 5×10^{-11} Torr. Pump-induced average heating of the sample has been estimated to be around 50–60 K, via fitting of the Fermi edge with a Fermi–Dirac distribution function convoluted with the

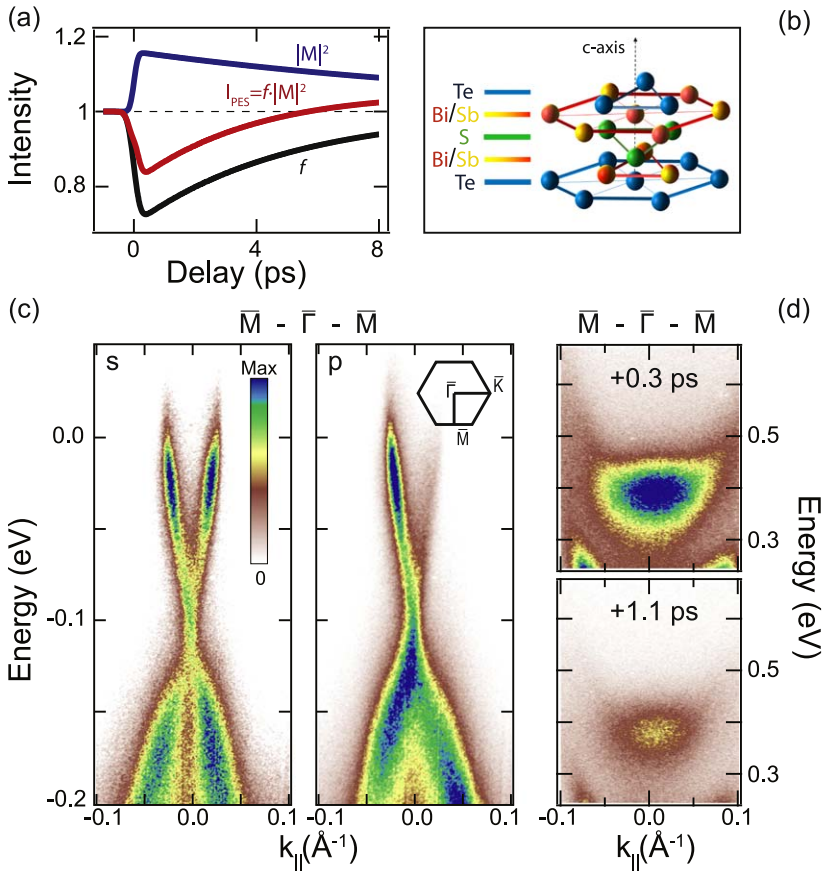

Figure 1. (a) Pictorial sketch of how a transient modification of the matrix element may affect the extraction of the intrinsic electron relaxation time from the evolution of the photoemission intensity: blue line, matrix element $|M|^2$, modeled as a single-exponential function with a decay time of 15 ps convoluted with a 0.25 ps Gaussian function, ≈15% maximum variation; black line, electronic distribution f, modeled as a single-exponential function with a decay time of 5 ps convoluted with a 0.4 ps Gaussian function, ≈−25% maximum variation; red line, photoemission intensity, $I_{PES} = f \cdot |M|^2$. (b) $Bi_{1.1}Sb_{0.9}Te_2S$ layered-crystal structure. (c) 6.2 eV ARPES maps for $\tau < 0$, along $\bar{\Gamma}$–$\bar{M}$, acquired at 6 K with vertically (s) and horizontally (p) polarized light. The inset shows the hexagonal projected Brillouin zone with two high-symmetry directions. (d) TR-ARPES mapping (s-polarization) of the conduction band along $\bar{\Gamma}$–$\bar{M}$ for +0.3 ps and +1.1 ps pump-probe delays.

energy resolution (see supplementary material available online at stacks.iop.org/NJP/22/023031/mmedia). The incident plane of the laser beams and the analyzer slit were aligned along $\bar{\Gamma}$–$\bar{M}$ direction.

We also performed high-temporal resolution TR-reflectivity to verify the presence of optically-active phonons (A_{1g} optical modes) which may induce transient modifications to the electronic structure. TR-reflectivity measurements (1 kHz repetition rate) were performed using a 2.25 eV pump, 3 mJ cm^{-2} incident fluence, and broadband near-infrared probe. Sub-20 fs pump and probe pulses (overall temporal resolution better than 30 fs) are sufficiently short to detect photoinduced phonons in the time domain [28].

3. Results

Similar to Bi_2Se_3/Te_3, the crystal structure of BSTS forms a quintuple-layer structure with alternating layers of Te–Bi/Sb–S–Bi/Sb–Te stacked along the lattice c-axis (figure 1(b)) [24]. Static ARPES, along the $\bar{\Gamma}$–$\bar{M}$ direction and acquired with both vertically (s) and horizontally (p) polarized 6.2 eV photons, confirms the presence of a metallic TSS, with the Dirac point (DP) located 120 meV below E_F (figure 1(c)). The multi-layer and -orbital structure of the wavefunction of the TSS leads to a characteristic angular modulation of the photoemission intensity, as a consequence of the interference between photoelectrons emitted from different layers and orbitals [29–34][13]. In the particular case of an isotropic Dirac-like TSS (not warped), the two branches of the TSS are

[13] The TSS wavefunction Ψ_{TSS} can be written as a linear combination of layer-dependent atomic orbitals η_τ ($\tau = \{p_x, p_z, \ldots\}$): $\Psi_{TSS}(\mathbf{k}) = \sum_{j,\tau} C^{\mathbf{k}}_{j,\tau} \eta_{j,\tau}(\mathbf{k})$, where j is the atomic layer index (sum over spin is suppressed for clarity) [29, 33, 34]. As already reported by Zhu *et al* [29], the photoemission matrix element can be written as $M^{\mathbf{k}}_{f,TSS} \propto \sum_{j,\tau} e^{-i\phi(z_j)} C^{\mathbf{k}}_{j,\tau} < \Psi_f(\mathbf{k}_\parallel) | \hat{H}^{pol}_{int} | \eta_{j,\tau} >$, where $\phi(z_j) = k_z \cdot z_j$ is a phase term accounting for interference effects among photoelectrons emitted from different layers stacked along z (c-axis).

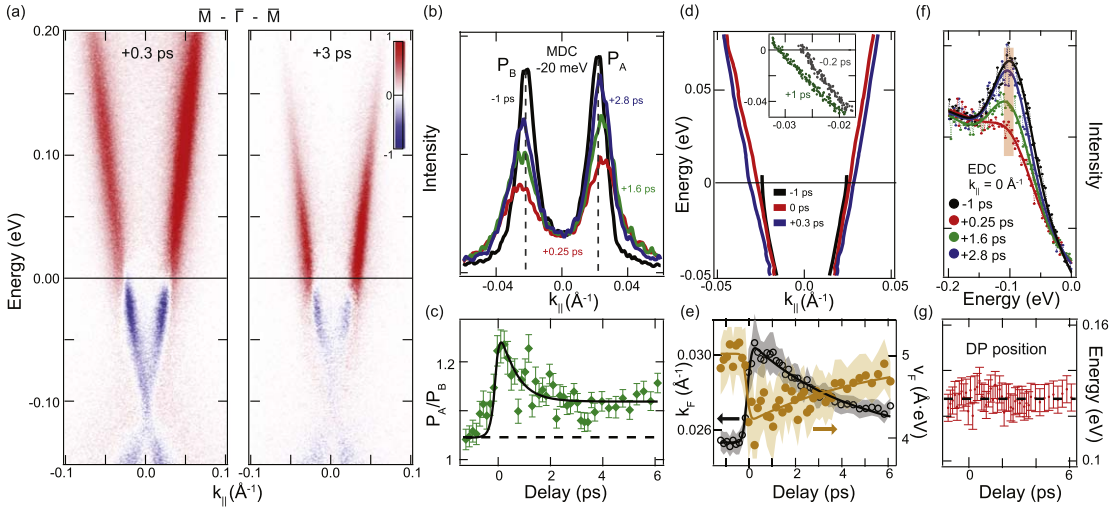

Figure 2. (a) Differential ($\mathrm{Pump}_{\tau>0} - \mathrm{Pump}_{\tau<0}$) band mapping of the TSS at +0.3 ps and +3 ps pump-probe delays, along $\bar{\Gamma}$–$\bar{\mathrm{M}}$, probed with s-polarized light. (b) Momentum distribution curves (MDCs) at −20 meV binding energy, s-polarized light, and different pump-probe delays. (c) Temporal evolution of the ratio between the spectral amplitude of the two branches of the TSS as probed with s-polarized light at −20 meV binding energy (P_A/P_B, as defined in (b), where P identifies the spectral area). The black solid line is a phenomenological bi-exponential decay function which shows that the modification of the relative intensity of the branches of the TSS lasts for delays $\tau > 6$ ps. Error bars are defined as ±1 standard deviation. (d) TSS dispersion extracted by a double-Lorentzian fit of the MDCs. The TSS dispersion changes upon the optical excitation. The inset highlights the transient modification of both the Fermi velocity and Fermi momentum by simple visual inspection. (e) Extracted Fermi velocity (v_F, filled orange circles) and Fermi momentum (k_F, open black circles) referred to the equilibrium E_F. Traces are fit by a phenomenological exponential decay function. (f) Energy distribution curves (EDCs) at $k = 0$ Å^{-1} for different pump-probe delays (s-polarization, filled circles). Solid lines are fit with a Gaussian and a polynomial background: the peak does not shift within an uncertainty of ±7.5 meV (red rectangular shadow). Note that the peak position (≈−100 meV) does not match the DP position (≈−120 meV) as a consequence of photoemission intensity pattern (see figure 1(c)). (g) DP position extrapolated from the temporal evolution k_F and v_F in (e): $E_{DP}(\tau) = k_F(\tau) \cdot v_F(\tau)$. The shadowed area in (e), the red rectangular shadow in (f), and error bars in (g), are defined as the 95% fitting confidence interval.

expected to have equal intensity when probed with s-polarized light—while the intensity of one branch is suppressed for p-polarized light—[29, 30], in agreement with our results.

We mapped the dispersion of the bulk conduction band via TR-ARPES along the $\bar{\Gamma}$–$\bar{\mathrm{M}}$ direction by introducing the 1.55 eV pump excitation (see figure 1(d)). The minimum of the conduction band is located at ≈0.35 eV, the value of which exceeds the minimum band gap reported in [24] as a consequence of the particular out-of-plane momentum probed by 6.2 eV light. Figure 1(d) confirms that our pump excitation populates unoccupied bulk states for approximately 1 ps, in agreement with previous TR-ARPES studies of TIs at similar or higher excitation fluence [10, 14–16, 25, 26, 35–44].

We now move our attention to the study of the TSS, and summarize the results of our TR-ARPES study in figure 2. The system's strong, and long-lasting response to the IR pump is seen clearly in figures 2(a) and 4(a), (b). In particular, figure 2(a) displays the differential ARPES spectra, where we plot the TSS along the $\bar{\Gamma}$–$\bar{\mathrm{M}}$ direction at 0.3 and 3 ps pump-probe delays, as probed with s-polarized light. We observe a dynamical redistribution of carriers, as well as a modification of both dispersion and relative intensity patterns (i.e. stemming from the photoemission matrix element). Regarding the intensity patterns, in figure 2(b) momentum distribution curves (MDCs) at −20 meV binding energy are plotted for representative pump-probe delays. While the MDC area ratio between left and right branches approaches unity prior to the pump-arrival, in agreement with what is expected for an isotropic Dirac-like TSS probed with s-polarized light [29], a marked asymmetry appears for longer delays (figure 2(c)). As in figures 2(b), (c) we consider intensity at the same binding energy and for symmetry-equivalent states, one would anticipate identical contributions from both the electronic distribution and spectral function. Any different evolution can then be attributed to the matrix elements. We return to these issues in the discussion below, where we corroborate our observation via a polarization-dependent study of the transient signal of the TSS (see figure 4).

In addition to this matrix-element dynamics, a pump-induced change in the spectral dispersion is observed; this is particularly well resolved in figure 2(d) and inset. The values of the Fermi surface area (i.e. the Fermi momentum k_F) and velocity (v_F) extracted from an MDC fitting procedure are summarized for all delays in figure 2(e). Such an observation requires consideration of the possible impact of photoinduced surface-photovoltage (SPV) effects, which have been reported widely in a variety of bulk-insulating TIs [36, 37, 41–44]. We note that SPV would induce a rigid band shift, instead of the polarization dependent photoemission intensity dynamics reported below and in figure 4, and would thus not affect our analysis and conclusions (see supplementary material available online at stacks.iop.org/NJP/22/023031/mmedia). Furthermore, even if we

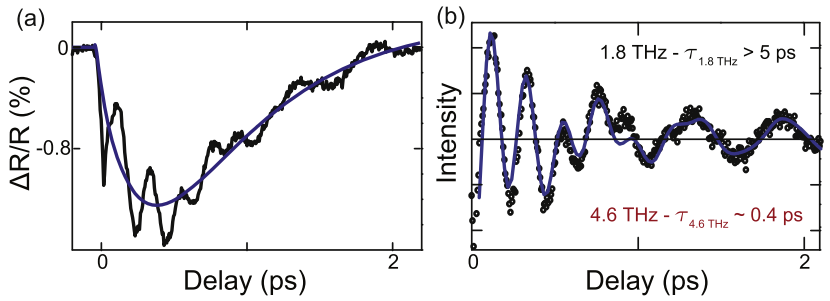

Figure 3. (a) Differential reflectivity $\Delta R(\tau)/R$ trace (black curve) at 300 K, pump 2.25 eV (incident fluence of 3 mJ cm^{-2}) and probe 1.37 eV. $\Delta R(\tau)/R$ trace is fit by a phenomenological bi-exponential decay function (blue line) extracting a rise time of 0.33 $\pm$ 0.05 ps and subsequent relaxation time of 0.65 $\pm$ 0.1 ps. (b) $\Delta R(\tau)/R$ curve subtracted by the bi-exponential fitting function shown in (a). The blue line is a double damped-sinusoidal function fit.

cannot exclude the presence of a minor SPV, we observe two effects at variance with what expected for a mere SPV: (i) a transient modification of v_F (figures 2(d)–(e)), and (ii) the DP to be stable to within our resolution. The stability of the DP is confirmed by both the energy distribution curves centered at $k = 0$ Å^{-1} (figure 2(f)), as well as the extrapolation of the DP position from the transient evolution of $v_F(\tau)$ and $k_F(\tau)$ (figures 2(e), (g)).

The photoinduced modification of the dispersion of the TSS is consistent with what has been reported by Sobota *et al* [19], who attributed it to a photoinduced lattice distortion, which affects the covalency for those states comprising the TSS. Such phonon excitations have been reported extensively for both TIs and other materials [19, 20]. Therefore, while the particular microscopic origin of the photoemission matrix elements dynamics is challenging to ascertain, in light of the observed evolution of the dispersion the excitation of phonons is a plausible candidate.

High time-resolution TR-reflectivity has been widely employed for studying photoinduced phonons. In particular, A_{1g} phonons with a frequency of a few THz have been commonly observed in TIs after a near-IR perturbation [45–51]. To confirm the presence of lattice vibrations photoinduced by the pump, we have thus performed a high time-resolution TR-reflectivity investigation of BSTS, which is so far missing to the best of our knowledge. Indeed figure 3 demonstrates the presence of two optical phonons: A^2_{1g} at 4.6 THz and A^1_{1g} at 1.79 THz [51] (note that the $\approx$250 fs temporal resolution of our TR-ARPES system prevents us to observe coherent oscillations of the band dispersion as reported in [19, 20]). A single trace of the recorded differential reflectivity $\Delta R(\tau)/R$ at probe energy 1.37 eV[14] is plotted in figure 3(a); subtracting the bi-exponential decay fit (see figure 3(b)), the residual curve can be fit to damped sinusoids from which we extract damping times of 0.4 ps (4.6 THz/19 meV) and >5 ps (1.79 THz/7.4 meV). We also note that additional modes, not observed via reflectivity, may also play a secondary role in establishing the modified dispersion over the timescale measured in our experiment [52]. It is thus plausible that the modifications to the TSS dispersion may be attributed to a complex interplay of several pump-induced phonons.

With the transient modification to the electronic structure confirmed, we now address the resulting changes to the ARPES matrix elements which ensue. To do so, we focus our attention on the temporal evolution of several well-defined regions of energy and momentum along the different branches of the TSS. While the ultrafast scattering processes involving the TSS of several TIs have been reported [10, 14–16, 25, 26, 35–44], the effect of changes of the electronic dispersion discussed above has not been addressed. In figure 4(a) we plot the TSS at +0.6 ps pump-probe delay for two different linear probe polarizations (s and p). The area of the integration regions indicated by the colored boxes in figure 4(a) was chosen to be comparable in energy to our system resolution (20 meV), and large enough in momentum so as to ensure that no states move in or out of the integration window with the change in dispersion. It is important to note that since the DP does not shift with the pump excitation (see figure 2), the energy window is fixed with respect to the TSS for all time delays. The temporal evolution of the integrated intensity within these boxes, $\Delta I(\tau) = \int_{\omega,\mathbf{k}} I_{\mathrm{PES}}(\omega, \mathbf{k}, \tau)\mathrm{d}\omega\mathrm{d}\mathbf{k}$, is then plotted in figure 4(b). Comparing this evolution for different energy windows on both the left (L) and right (R) branches of the Dirac cone with s- and p-polarized probe light, we find that, remarkably, $\Delta I(\tau)$ depends on the choice of probe polarization. We repeat that the pump polarization is fixed, and so this observation can not be explained as the result of different excitation channels associated with variations in the pump. Furthermore, as we probe only a single TSS within a given integration window, the observed differences in relaxation rates cannot be attributed to either $f(\omega, \mathbf{k}, \tau)$ or $A(\omega, \mathbf{k}, \tau)$, because these have no connection within this context to the probe pulse polarization. Rather it would seem that the matrix elements exhibit distinct temporal evolution that

[14] Other probe photon energies show a similar behavior.

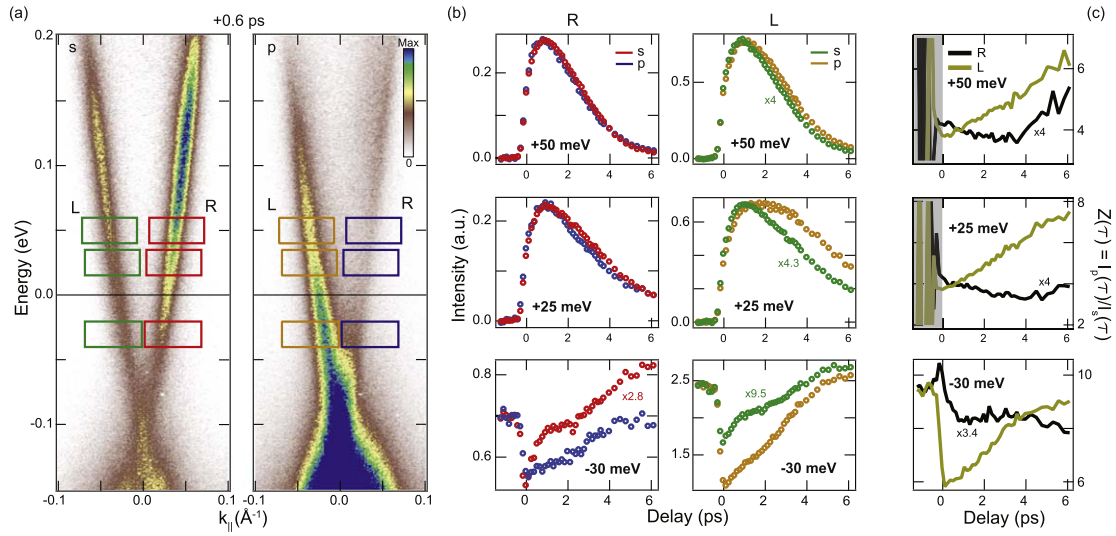

Figure 4. (a) Out-of-equilibrium band mapping of the TSS, +0.6 ps pump-probe delay, probed with s (left) and p (right) polarizations. In each panel, the color scale highlights the regions of interest of this study. (b) $\Delta I(\tau)$ curves centered at +50, +25 and −30 meV resulting from the integration in colored boxes in (a). Red and blue curves: s and p polarizations, right (R) branch; green and orange curves: s and p polarizations, left (L) branches. (c) Temporal evolution of $Z(\tau)$ as defined in equation (2).

depends on the choice of probe polarization. In addition, we note that the $\Delta I(\tau)$ curves at −30 meV binding energy in figure 4(b) show similar behavior to the model discussed in figure 1(a), i.e. the photoemission intensity exceeds its equilibrium value for late delays. This observation further confirms the dominant role of dynamical matrix elements in driving the evolution of the photoemission intensity.

4. Discussion

We can gain more explicit information regarding the photoemission matrix element dynamics via evaluation of:

$$Z(\tau) = (I_p/I_s)(\tau) = |M_p(\tau)|^2/|M_s(\tau)|^2. \quad (2)$$

This quantity is defined as the ratio between photoemission intensities with p- and s-polarized light. The form of $Z(\tau)$ has been chosen to eliminate contributions from both $A(\omega, \mathbf{k}, \tau)$ and $f(\omega, \mathbf{k}, \tau)$, retaining only the relative matrix element dynamics (note that this is valid even beyond the dipole-approximation commonly employed for describing photoemission matrix elements). In the absence of temporal evolution for $|M(\tau)|^2$, or for equivalent time dependence in both polarization channels, $Z(\tau)$ would be constant. In figure 4(c), we plot $Z(\tau)$ as a function of the pump-probe delay for three different binding energies: two above the equilibrium chemical potential (+50 and +25 meV), and one below (−30 meV). As exemplified by the lower panel, the matrix elements undergo an ultrafast response and subsequent relaxation, following the interaction with the pump. For all three binding energies, we observe a transient evolution of $Z(\tau)$, unambiguously related to a dynamical matrix element ratio.

We also observe a strong dependence of $Z(\tau)$ on both momentum and energy, with the distinction between *s* and *p* polarized light seen primarily along the left branch. Ultimately, the microscopic origin of the matrix element dynamics in BSTS is beyond the scope of this work. Our primary objective is to demonstrate the important consequences of $Z(\tau)$ when characterizing the ultrafast response of the spectral and distribution functions. The particular form of $Z(\tau)$ could stem from pump-induced modifications to the initial state wavefunction, warping of the Dirac cone, or even the nature of the photoemission final states. In the present context, one plausible contribution may derive from the commonly reported photoinduced A_{1g} optical phonons in TIs (see figure 3 and [19, 49, 51, 53]). These out of plane modes, i.e. along the *c*-axis, may induce a transient modification of the relative distance between atomic-layers, modulating the initial and final state wavefunctions, as well as the phase difference between electrons emitted from different atomic layers. Such photoinduced modulations may result in an energy- and momentum-dependent modification of the photoemission intensity [29–34], similar to what has been observed here (see figure 2(c) and figure 4). Finally, we note that the pump-induced anisotropy of the photoemission intensity reported in figure 2(c) persists out to long delay times ($\tau > 6$ ps), ruling out intermediate/virtual state contributions which may play a role in two-photon-photoemission processes, and once again suggesting a long-lived microscopic origin such as lattice distortions.

Beyond this photoinduced vibration scenario, we recognize that other mechanisms may play a role in the modification of the TSS and the associated dynamics of matrix elements, such as the ultrafast modification of the screening [54], photoinduced effective mass renormalization [55], or coupling to other bosonic modes (e.g. plasmons [56]). The variety of plausible contributions to $Z(\tau)$ highlights the theoretical challenge presented by a more thorough consideration of dynamical matrix elements in TR-ARPES experiments. These need to be taken into account in order to ensure the successful application of this technique to the quantitative study of topological insulators and other materials.

5. Conclusion

We have reported a substantial photoinduced modification of the electronic structure of the topological insulator BSTS. This response is manifest in corrections to both the electronic dispersion and eigenstates. We discussed the scenario where both $A(\omega, \mathbf{k}, \tau)$ and $|M^{\mathbf{k}}_{\mathrm{f,i}}(\tau)|^2$ display dynamic behavior, and emphasized the corresponding implications for the interpretation of TR-ARPES experiments. We showed here that a probe-polarization study can be used to reveal a time-dependence or lack-thereof within the different $|M^{\mathbf{k}}_{\mathrm{f,i}}(\tau)|^2$ channels. Isolating the dynamics of the dipole matrix elements is a critical, necessary step towards the comprehensive understanding of the non-equilibrium properties of complex solid state systems by TR-ARPES.

Acknowledgments

We gratefully thank H.-H. Kung for fruitful discussions. This research was undertaken thanks in part to funding from the Max Planck-UBC-UTokyo Centre for Quantum Materials and the Canada First Research Excellence Fund, Quantum Materials and Future Technologies Program. This project was supported by: the Gordon and Betty Moore Foundation's EPiQS Initiative, Grant GBMF4779 to AD and DJJ; the Killam, Alfred P Sloan, and Natural Sciences and Engineering Research Council of Canada's (NSERC's) Steacie Memorial Fellowships (AD); the Alexander von Humboldt Fellowship (AD); the Canada Research Chairs Program (AD); NSERC, Canada Foundation for Innovation (CFI); British Columbia Knowledge Development Fund (BCKDF); and CIFAR Quantum Materials Program. ER acknowledges support from the Swiss National Science Foundation (SNSF) grant no. P300P2_164649. CG acknowledge financial support from MIUR through the PRIN 2015 Programme (Prot. 2015C5SEJJ001) and from Università Cattolica del Sacro Cuore through D.1, D.2.2 and D.3.1 grants. This project has received funding from the European Union's Horizon 2020 research and innovation programme under grant agreement 785219 GrapheneCore2. SKK acknowledges support of the LANL Directors Postdoctoral Funding LDRD program XWVM and US Department of Energy Office of Science, BESMSE Science of 100 Tesla programs.

ORCID iDs

F Boschini https://orcid.org/0000-0003-3503-9389
D Bugini https://orcid.org/0000-0002-2727-9406
M Zonno https://orcid.org/0000-0003-0668-5146
R P Day https://orcid.org/0000-0001-7292-0103
E Razzoli https://orcid.org/0000-0002-8893-972X
B Zwartsenberg https://orcid.org/0000-0002-9635-9039
M Schneider https://orcid.org/0000-0003-1955-1382
E H da Silva Neto https://orcid.org/0000-0001-6902-6100
S dal Conte https://orcid.org/0000-0001-8582-3185
S K Kushwaha https://orcid.org/0000-0002-3169-969X
S Zhdanovich https://orcid.org/0000-0002-0673-5089
A K Mills https://orcid.org/0000-0002-6629-5919
G Levy https://orcid.org/0000-0003-2980-0805
E Carpene https://orcid.org/0000-0003-3867-8178
C Dallera https://orcid.org/0000-0001-6981-2451
C Giannetti https://orcid.org/0000-0003-2664-9492
D J Jones https://orcid.org/0000-0002-4508-5912
G Cerullo https://orcid.org/0000-0002-9534-2702
A Damascelli https://orcid.org/0000-0001-9895-2226

References

[1] Giannetti C, Capone M, Fausti D, Fabrizio M, Parmigiani F and Mihailovic D 2016 *Adv. Phys.* **65** 58
[2] Boschini F *et al* 2018 *Nat. Mater.* **17** 416
[3] Smallwood C L, Hinton J P, Jozwiak C, Zhang W, Koralek J D, Eisaki H, Lee D-H, Orenstein J and Lanzara A 2012 *Science* **336** 1137
[4] Rettig L, Cortés R, Jeevan H S, Gegenwart P, Wolf T, Fink J and Bovensiepen U 2013 *New J. Phys.* **15** 083023
[5] Rohwer T *et al* 2011 *Nature* **471** 490
[6] Mor S *et al* 2017 *Phys. Rev. Lett.* **119** 086401
[7] Wang Y H, Steinberg H, Jarillo-Herrero P and Gedik N 2013 *Science* **342** 453
[8] Mahmood F, Chan C-K, Alpichshev Z, Gardner D, Lee Y, Lee P A and Gedik N 2016 *Nat. Phys.* **12** 306
[9] Sterzi A, Crepaldi A, Cilento F, Manzoni G, Frantzeskakis E, Zacchigna M, van Heumen E, Huang Y K, Golden M S and Parmigiani F 2016 *Phys. Rev.* B **94** 081111
[10] Sterzi A, Manzoni G, Sbuelz L, Cilento F, Zacchigna M, Bugnon P, Magrez A, Berger H, Crepaldi A and Parmigiani F 2017 *Phys. Rev.* B **95** 115431
[11] Perfetti L, Loukakos P A, Lisowski M, Bovensiepen U, Eisaki H and Wolf M 2007 *Phys. Rev. Lett.* **99** 197001
[12] Boschini F *et al* 2020 *npj Quantum Mater.* **5** 6
[13] Crepaldi A *et al* 2017 *Phys. Rev.* B **96** 241408
[14] Hajlaoui M *et al* 2012 *Nano Lett.* **12** 3532
[15] Sobota J A, Yang S, Analytis J G, Chen Y L, Fisher I R, Kirchmann P S and Shen Z-X 2012 *Phys. Rev. Lett.* **108** 117403
[16] Bugini D, Boschini F, Hedayat H, Yi H, Chen C, Zhou X, Manzoni C, Dallera C, Cerullo G and Carpene E 2017 *J. Phys.: Condens. Matter* **29** 30LT01
[17] Damascelli A 2004 *Phys. Scr.* **2004** 61
[18] Randi F, Fausti D and Eckstein M 2017 *Phys. Rev.* B **95** 115132
[19] Sobota J A, Yang S-L, Leuenberger D, Kemper A F, Analytis J G, Fisher I R, Kirchmann P S, Devereaux T P and Shen Z-X 2014 *Phys. Rev. Lett* **113** 157401
[20] Gerber S *et al* 2017 *Science* **357** 71
[21] Na M *et al* 2019 *Science* **366** 1231
[22] Perfetti L, Loukakos P, Lisowski M, Bovensiepen U, Wolf M, Berger H, Biermann S and Geroges A 2018 *New J. Phys* **10** 053019
[23] Freericks J and Krishnamurthy H 2016 *Photonics* **3** 58
[24] Kushwaha S K *et al* 2016 *Nat. Commun.* **7** 11456
[25] Kuroda K, Reimann J, Güdde J and Höfer U 2016 *Phys. Rev. Lett.* **116** 076801
[26] Sánchez-Barriga J, Scholz M R, Golias E, Rienks E, Marchenko D, Varykhalov A, Yashina L V and Rader O 2014 *Phys. Rev.* B **90** 195413
[27] Sobota J A *et al* 2013 *Phys. Rev. Lett.* **111** 136802
[28] Brida D, Bonora S, Manzoni C, Marangoni M, Villoresi P, Silvestri S D and Cerullo G 2009 *Opt. Express* **17** 12510
[29] Zhu Z-H, Veenstra C N, Levy G, Ubaldini A, Syers P, Butch N P, Paglione J, Haverkort M W, Elfimov I S and Damascelli A 2013 *Phys. Rev. Lett.* **110** 216401
[30] Zhu Z-H *et al* 2014 *Phys. Rev. Lett.* **112** 076802
[31] Gierz I, Henk J, Höchst H, Ast C R and Kern K 2011 *Phys. Rev. B* **83** 121408
[32] Liu Y, Bian G, Miller T and Chiang T-C 2011 *Phys. Rev. Lett.* **107** 166803
[33] Bawden L *et al* 2015 *Sci. Adv.* **1** e1500495
[34] Cao Y *et al* 2013 *Nat Phys.* **9** 499
[35] Sobota J, Yang S-L, Leuenberger D, Kemper A, Analytis J, Fisher I, Kirchmann P, Devereaux T and Shen Z-X 2014 *J. Electron. Spectrosc. Relat. Phenom.* **195** 249
[36] Hajlaoui M *et al* 2014 *Nat. Commun.* **5** 4003
[37] Neupane M *et al* 2015 *Phys. Rev. Lett.* **115** 116801
[38] Sánchez-Barriga J, Golias E, Varykhalov A, Braun J, Yashina L V, Schumann R, Minár J, Ebert H, Kornilov O and Rader O 2016 *Phys. Rev.* B **93** 155426
[39] Jozwiak C, Sobota J A, Gotlieb K, Kemper A F, Rotundu C R, Birgeneau R J, Hussain Z, Lee D-H, Shen Z-X and Lanzara A 2016 *Nat. Commun.* **7** 13143
[40] Freyse F, Battiato M, Yashina L V and Sánchez-Barriga J 2018 *Phys. Rev.* B **98** 115132
[41] Sánchez-Barriga J, Battiato M, Golias E, Varykhalov A, Yashina L V, Kornilov O and Rader O 2017 *Appl. Phys. Lett.* **110** 141605
[42] Sumida K *et al* 2017 *Sci. Rep.* **7** 14080
[43] Yoshikawa T, Ishida Y, Sumida K, Chen J, Kokh K A, Tereshchenko O E, Shin S and Kimura A 2018 *Appl. Phys. Lett.* **112** 192104
[44] Papalazarou E *et al* 2018 *Phys. Rev. Mater.* **2** 104202
[45] Qi J *et al* 2010 *Appl. Phys. Lett.* **97** 182102
[46] Kumar N, Ruzicka B A, Butch N P, Syers P, Kirshenbaum K, Paglione J and Zhao H 2011 *Phys. Rev.* B **83** 235306
[47] Chen H-J *et al* 2012 *Appl. Phys. Lett.* **101** 121912
[48] Glinka Y D, Babakiray S, Johnson T A, Bristow A D, Holcomb M B and Lederman D 2013 *Appl. Phys. Lett.* **103** 151903
[49] Boschini F *et al* 2015 *Sci. Rep.* **5** 15304
[50] Choi Y G, Zhung C J, Park S-H, Park J, Kim J S, Kim S, Park J and Lee J S 2018 *Phys. Rev.* B **97** 075307
[51] Mondal R, Arai A, Saito Y, Fons P, Kolobov A V, Tominaga J and Hase M 2018 *Phys. Rev.* B **97** 144306
[52] Bykov A Y, Murzina T V, Olivier N, Wurtz G A and Zayats A V 2015 *Phys. Rev.* B **92** 064305
[53] Richter W and Becker C R 1977 *Phys. Status Solidi* b **84** 619
[54] Huber R, Tauser F, Brodschelm A, Bichler M, Abstreiter G and Leitenstorfer A 2001 *Nature* **414** 286
[55] Montagnese M, Pagliara S, Galimberti G, Dal Conte S, Ferrini G, van Loosdrecht P H M and Parmigiani F 2006 *Sci. Rep.* **6** 35318
[56] Basak A K, Petek H, Ishioka K, Thatcher E M and Stanton C J 2015 *Phys. Rev.* B **91** 125201